Supplementary Information: Anomalous and normal dislocation modes in Floquet topological insulators

Tanay Nag[1,2] and Bitan Roy[3]

[1]*SISSA, via Bonomea 265, 34136 Trieste, Italy*
[2]*Institute für Theorie der Statistischen Physik, RWTH Aachen University, 52056 Aachen, Germany*
[3]*Department of Physics, Lehigh University, Bethlehem, Pennsylvania, 18015, USA*
(Dated: June 4, 2021)

Supplementary Note 1.   DISLOCATION MODES IN A 2D STATIC TOPOLOGICAL INSULATOR

The Hamiltonian describing a time-reversal symmetry breaking two-dimensional (2D) static topological insulator reads $H = \sum_{\mathbf{k}} \Psi_{\mathbf{k}}^{\dagger} \hat{h}(\mathbf{k}) \Psi_{\mathbf{k}}$, where $\Psi_{\mathbf{k}}$ is a two-component spinor and $\hat{h}(\mathbf{k}) = \sigma_{\alpha} d_{\alpha}(\mathbf{k})$. Here summation over repeated index $\alpha = 0, \cdots, 3$ is assumed, and

$$\mathbf{d}(\mathbf{k}) = (d_1(\mathbf{k}), d_2(\mathbf{k}), d_3(\mathbf{k})) = \left(t_1 \sin(k_x a), t_1 \sin(k_y a), m_0 - t_0 \sum_{j=x,y} \cos(k_j a) \right). \tag{S1}$$

Hereafter we set the lattice spacing $a = 1$. As the particle-hole asymmetry $d_0(\mathbf{k})$ plays no role in topology in static or dynamic systems, we throughout set $d_0(\mathbf{k}) = 0$ from the outset. In principle, one can incorporate a nontrivial $d_0(\mathbf{k})$, while studying Chern insulators for charge fermions by taking $d_0(\mathbf{k}) = [m + t\{\cos(k_x a) + \cos(k_y a)\}]$. By contrast, in a $p_x + i p_y$ superconductor $d_0(\mathbf{k}) \equiv 0$ (identically) due to the charge conjugation symmetry. Addition of the particle-hole asymmetry in a Chern insulator only causes an overall shift in energy, without altering the band inversion momentum $\mathbf{K}_{\text{inv}}$ that in turn determine the momentum at which the counter propagating one-dimensional edge modes cross each other and the phase acquired by an electron while encircling the dislocation core $\Phi_{\text{dis}}^{\text{top}} = \mathbf{K}_{\text{inv}} \cdot \mathbf{b}$ (modolu 2π). Consequently, the topological edge and dislocation modes remain unaffected by the particle-hole asymmetry, besides suffering a trivial shift in energy. Notice that dislocation modes appear at energy at which counter propagating edge modes cross each other at $k_x = \pi$ or $k_y = \pi$ (resulting from finite momentum band inversion).

As mentioned in the main text that this model supports topological and trivial insulators (both electrical and thermal) respectively for $|m_0/t_0| < 2$ and $|m_0/t_0| > 2$. Moreover, within the topological regime there are two distinct insulating phases. Namely, (a) the Γ phase, featuring band inversion at the $\Gamma = (0,0)$ point of the Brillouin zone (BZ) and (b) the M phase, where the band inversion takes place at the $M = (\pi, \pi)$ point. Respectively, these two phases are found for $0 < m_0/t_0 < 2$ and $-2 < m_0/t_0 < 0$. Here we focus on the M phase. As shown in Fig. S1(a), the corresponding edge modes are indeed found near $k_x = \pi$ in a semi-infinite system with k_x as a good quantum number, but with open boundaries in the y direction. These conclusions remain unchanged when we add a particle-hole symmetry breaking term like $t_x \sin(k_x a) \sigma_3$ or $t_y \sin(k_y a) \sigma_3$, with t_x or t_y as large as 1. Namely, the edge modes are found at $k_x = 0$ (π) when $0 < m_0/t_0 < 2$ $(-2 < m_0/t_0 < 0)$. As a result the dislocation modes are found for $-2 < m_0/t_0 < 0$ when the Burgers vectors of the dislocation defects are $\mathbf{b} = \pm a \mathbf{e}_x$.

Next we diagonalize the above Hamiltonian with a pair of edge dislocation-antidislocation and search for the zero-energy modes, bound to the dislocation core in the M phase. To this end, we implement the above tight-binding model in the real space by using the Fourier transformation which in the presence of a single edge dislocation reads

$$\hat{h}_{\text{real}} = \Bigg(\Bigg[\left\{ \left(\sum_{n_x=1}^{\ell_x-2} \sum_{n_y=1}^{\ell_y-1} + \sum_{n_x=\ell_x+1}^{L_x-1} \sum_{n_y=1}^{\ell_y-1} + \sum_{n_x=1}^{L_x-1} \sum_{n_y=\ell_y}^{L_y} \right) c_{n_x,n_y}^{\dagger} c_{n_x+1,n_y} \right\} \otimes \frac{i t_1 \sigma_1 - t_0 \sigma_3}{2} $$
$$+ \left\{ \left(\sum_{n_x=1}^{\ell_x-1} \sum_{n_y=1}^{L_y-1} + \sum_{n_x=\ell_x+1}^{L_x} \sum_{n_y=1}^{L_y-1} \right) c_{n_x,n_y}^{\dagger} c_{n_x,n_y+1} + \sum_{n_y=\ell_y}^{L_y-1} c_{\ell_x,n_y}^{\dagger} c_{\ell_x,n_y+1} \right\} \otimes \frac{i t_1 \sigma_2 - t_0 \sigma_3}{2} \Bigg] + H.c. \Bigg) $$
$$+ \sum_{j=1}^{L_x L_y - (\ell_y-1)} c_{j,j}^{\dagger} c_{j,j} \otimes m_0 \, \sigma_3 + \left(\sum_{n_y=1}^{\ell_y} c_{\ell_x-1,n_y}^{\dagger} c_{\ell_x+1,n_y} \right) \otimes \frac{i t_1' \sigma_1 - t_0' \sigma_3}{2}. \tag{S2}$$
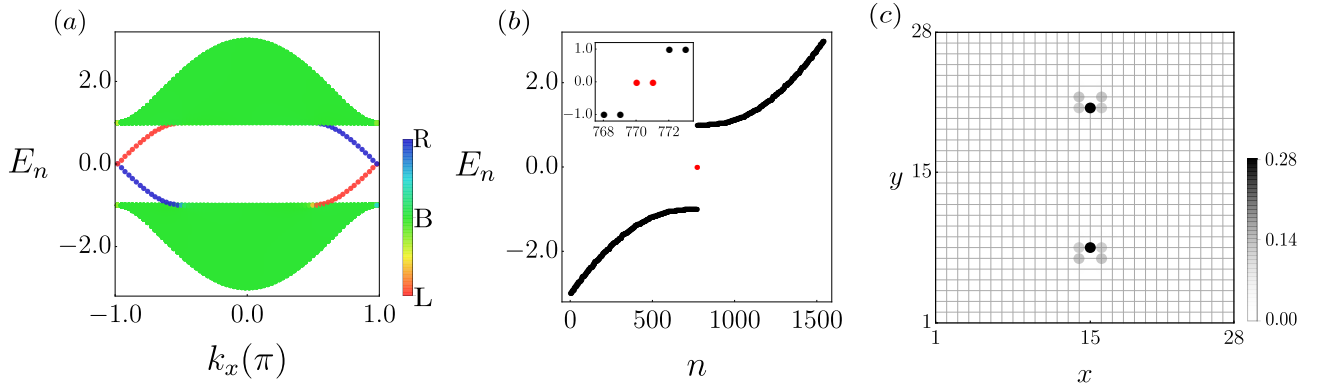
Figure S1: Dislocation as a bulk probe of a static topological insulator with the Chern number $C = 1$. (a) Energy (E_n) spectra in a semi-infinite system (with k_x as a good quantum number) of linear dimension $L = 100$ in the y direction (with open boundaries) for $t_1 = t_0 = -m_0 = 1.0$ (yielding the M phase). Here blue and red [green] states are localized on the right (R) and left (L) edges [in the bulk (B)] of the system, respectively, confirming that the band inversion takes place at $k_x = \pi$. (b) The zero energy ($E_n = 0$) dislocation modes (red), well separated from the bulk states (black), in a periodic system with a pair of edge dislocation-antidislocation with the Burgers vector $\mathbf{b} = \pm a\mathbf{e}_x$. (c) Local density of states (LDoS) of the dislocation modes. This situation is qualitatively similar to the FTI with $C = +1$ in the high frequency regime (Fig. 3 of the main text).

Here $c_{i,j}$ ($c_{i,j}^\dagger$) is the fermion annihilation (creation) operator at site (i, j). In this construction, the core of the edge dislocation is located at (ℓ_x, ℓ_y) [see Fig. 1 of the main text]. This construction can be generalized to implement a pair of edge dislocation-antidislocation with periodic boundaries. Hopping amplitudes across the line of missing atoms ending at the dislocation core are t_1' and t_0'. However, for simplicity, throughout we set $t_1' = t_1$ and $t_0' = t_0$.

In Fig. S1(b) we display the energy spectra in such a system, showing the existence of two modes at (almost) zero energy (red dots), which are well separated from the bulk states (black dots). Furthermore, the spatial profile of the local density of states (LDoS) shows that these two modes are highly localized near the center of the pair of edge dislocation-antidislocation, see Fig. S1(c). Hence, the M phase is translationally active in a 2D static topological insulator. By contrast, the Γ phase supports edge modes near $k_x = 0$ and does not lead to any dislocation modes near the zero energy. Whereas in a static trivial insulator there is no edge mode to begin with. We follow the same procedure while scrutinizing the response of any Floquet insulator to dislocation.

It should be noted that the dislocation modes are solely guaranteed by the nontrivial π (modulo 2π) phase acquired by electrons while encircling its core whenever the band inversion takes place at finite momentum in both static and Floquet systems. The modified hopping amplitudes [t_1' and t_0' in Eq. (S2)] due to the distortion of the bonds across the line of missing atoms (see Fig. 1 of main text) does not affect their stability. For concreteness, we set $t_1' = t_1/2$ and $t_0' = t_0/2$, assuming that the bonds across the line of missing atoms are twice longer than those in the rest of the system and show that dislocation modes remain qualitatively unaffected by this modification. See Fig. S2. Any reasonable profile of the hopping amplitudes around the dislocation core leaves the outcomes qualitatively unaffected.

Supplementary Note 2.   FLOQUET OPERATOR AND FLOQUET HAMILTONIAN

In this section we present details of the Floquet or time evolution operator $U(\mathbf{k}, T)$ and the corresponding Floquet Hamiltonian $\hat{h}_{\mathrm{Flq}}(\mathbf{k})$. When a static system, described by the Hamiltonian $\hat{h}(\mathbf{k})$, is periodically driven by the perturbation $\hat{V}(t)$ [Eqs. (1) and (3) of main text], the corresponding time evolution operator after a single kick reads

$$U(\mathbf{k}, T) = \mathrm{TO}\left(\exp\left[-i\int_0^T \left[\hat{h}(\mathbf{k}) + \hat{V}(t)\right] dt\right]\right) = \exp(-im_1\sigma_3)\exp(-i\hat{h}(\mathbf{k})T) \equiv \exp\left(-iT\hat{h}_{\mathrm{Flq}}(\mathbf{k})\right). \quad \text{(S3)}$$

Here 'TO' stands for time-ordered product. The effective Floquet Hamiltonian $\hat{h}_{\mathrm{Flq}}(\mathbf{k}) = \boldsymbol{\sigma} \cdot \mathbf{d}_{\mathrm{Flq}}(\mathbf{k})$, assumes the form of its static counterpart $\hat{h}(\mathbf{k})$, however, in terms of the $\mathbf{d}_{\mathrm{Flq}}(\mathbf{k})$ vector, given by $\mathbf{d}_{\mathrm{Flq}}(\mathbf{k}) = d_0(\mathbf{k})\mathbf{d}'(\mathbf{k})$, where

$$d_0(\mathbf{k}) = \frac{1}{T}\mathrm{Arccos}\left(A - D\frac{d_3(\mathbf{k})}{|\mathbf{d}(\mathbf{k})|}\right), \quad d_1'(\mathbf{k}) = \frac{d_0(\mathbf{k})}{\sin(d_0(\mathbf{k})T)}\left(B\frac{d_1(\mathbf{k})}{|\mathbf{d}(\mathbf{k})|} - D\frac{d_2(\mathbf{k})}{|\mathbf{d}(\mathbf{k})|}\right),$$
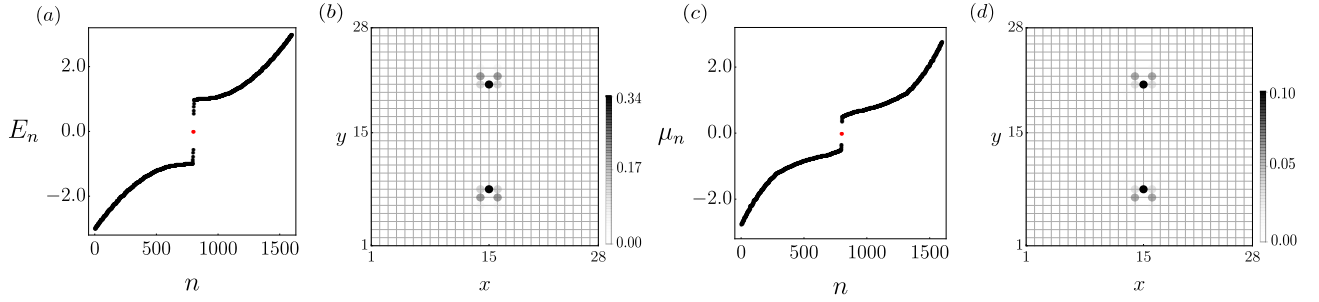
Figure S2: Stability of the dislocation modes in static [(a) and (b)] and Flqouet [(c) and (d)] systems against the modification of the hopping amplitudes along the distorted bonds across the line of missing atoms ending at the dislocation core. (a) Energy (E_n) spectra with a pair of edge dislocation-antidislcoation in a static system for $m_0 = -1$ [see Eq. (S1)]. (b) Local density of states (LDoS) for the zero energy dislocation modes [shown in red in (a)]. (c) Quasienergy (μ_n) spectra for a Floquet topological insulator with a dislocation-antidislocation pair for drive frequency $\omega = 12.9$, amplitude $m_1 = -1.84$, and $m_0 = 3$. (d) LDoS corresponidng to the normal dislocation mode at zero quasienergy [shown in red in (c)]. Throughout we set $t_1 = t_0 = 1$ and $t_1' = t_0' = 1/2$ [see Eq. (S2)]. The anomalous dislocation modes in Floquet insulators are also stable against such a modification of the hopping amplitudes across the sites of the missing atoms.

$$d_2'(\mathbf{k}) \; = \; \frac{d_0(\mathbf{k})}{\sin(d_0(\mathbf{k})T)} \left(B \, \frac{d_2(\mathbf{k})}{|\boldsymbol{d}(\mathbf{k})|} + D \, \frac{d_1(\mathbf{k})}{|\boldsymbol{d}(\mathbf{k})|} \right), \quad d_3'(\mathbf{k}) = \frac{d_0(\mathbf{k})}{\sin(d_0(\mathbf{k})T)} \left(B \, \frac{d_3(\mathbf{k})}{|\boldsymbol{d}(\mathbf{k})|} + C \right), \tag{S4}$$

with $|\mathbf{d}(\mathbf{k})| = \sqrt{d_1^2(\mathbf{k}) + d_2^2(\mathbf{k}) + d_3^2(\mathbf{k})}$ and

$$A = \cos(|\boldsymbol{d}(\mathbf{k})|T) \, \cos m_1, \quad B = \sin(|\boldsymbol{d}(\mathbf{k})|T) \, \cos m_1, \quad C = \cos(|\boldsymbol{d}(\mathbf{k})|T) \, \sin m_1, \quad D = \sin(|\boldsymbol{d}(\mathbf{k})|T) \, \sin m_1. \tag{S5}$$

We compute the Chern number C [Eq. (2) of the main text] from the components of the $\mathbf{d}_{\mathrm{Flq}}(\mathbf{k})$ vector to construct the global phase diagram of the time-reversal symmetry breaking Floquet insulators. See Fig. 2 of the main text.

It should noted that here we construct the effective Floquet Hamiltonian from Eq. (S3) solely for the purpose of computing the Chern number of Floquet insulators. However, all the analysis related to the dislocation modes are performed by diagonalizing the time evolution or the Flqouet operator, which only contains sort-range (namely, nearest-neighbor hopping and onsite staggered potential) terms. Therefore, it is much more feasible to implement and analyze the Flqouet operators, as often done in experiments. By contrast, the Floquet Hamiltonian contains longer range hopping [see Eq. (S4)], which are typically quite challenging to realize or implement in practice. Nevertheless, in the high frequency regime the Flqouet Hamiltonian simplifies considerably. In the high frequency limit $\omega \to \infty$ and $m_1 \to 0$, such that the ratio $m_1 \omega$ remains finite. Then $\cos m_1 \to 1$, $\sin m_1 \to m_1$, $\cos(|\boldsymbol{d}|T) \to 1$ and $\sin(|\boldsymbol{d}|T) \to |\boldsymbol{d}|T$, yielding $A \simeq 1$, $B \simeq |\boldsymbol{d}|T$, $C \simeq m_1$, $D \simeq |\boldsymbol{d}|Tm_1$. With these approximations $\mathbf{d}'(\mathbf{k})$ from Eq. (S4) becomes

$$d_1'(\mathbf{k}) \to \tilde{d}_1'(\mathbf{k}) \simeq d_1(\mathbf{k}) - d_2(\mathbf{k})m_1, \quad d_2'(\mathbf{k}) \to \tilde{d}_2'(\mathbf{k}) \simeq d_2(\mathbf{k}) + d_1(\mathbf{k})m_1, \quad d_3'(\mathbf{k}) \to \tilde{d}_3'(\mathbf{k}) \simeq d_3(\mathbf{k}) + \frac{m_1}{T}. \tag{S6}$$

The $\tilde{\mathbf{d}}'(\mathbf{k})$ vector can then be expressed compactly in term of the parameters from the lattice Hamiltonian as

$$\tilde{d}_1'(\mathbf{k}) = t_1 \sin k_x - t_1' \sin k_y, \quad \tilde{d}_2'(\mathbf{k}) = t_1' \sin k_x + t_1 \sin k_y, \quad \tilde{d}_3'(\mathbf{k}) = \left(m + \frac{m_1}{T} - t_0 \cos k_x - t_0 \cos k_y \right), \tag{S7}$$

where, $t_1' = t_1 m_1$. As in the high frequency regime the effective Floquet Hamiltonian $\hat{h}_{\mathrm{Flq}}^{\mathrm{HF}} = \boldsymbol{\sigma} \cdot \tilde{d}'(\mathbf{k})$, contains only local or short-range terms, it can be directly engineered in metamaterials, for example, at least in principle.

Supplementary Note 3.   FLOQUET INSULATORS WITHOUT DISLOCATION MODES

In this section we discuss the situations in Floquet topological insulators (FTIs) and Floquet trivial insulators that on the other hand do not support any dislocation modes. As we find either such states only support edge modes near $k_x = 0$ (resulting from Floquet-Bloch band inversion only at the Γ point of the BZ) or no edge modes at all. These examples in turn allow us to attribute both normal and anomalous dislocation modes solely to the Floquet-Bloch band inversion taking place near the M point of the BZ, which can occur at the Floquet zone center and/or boundary. This purpose is best served when we focus on the high frequency regime. The results are shown in Fig. S3.
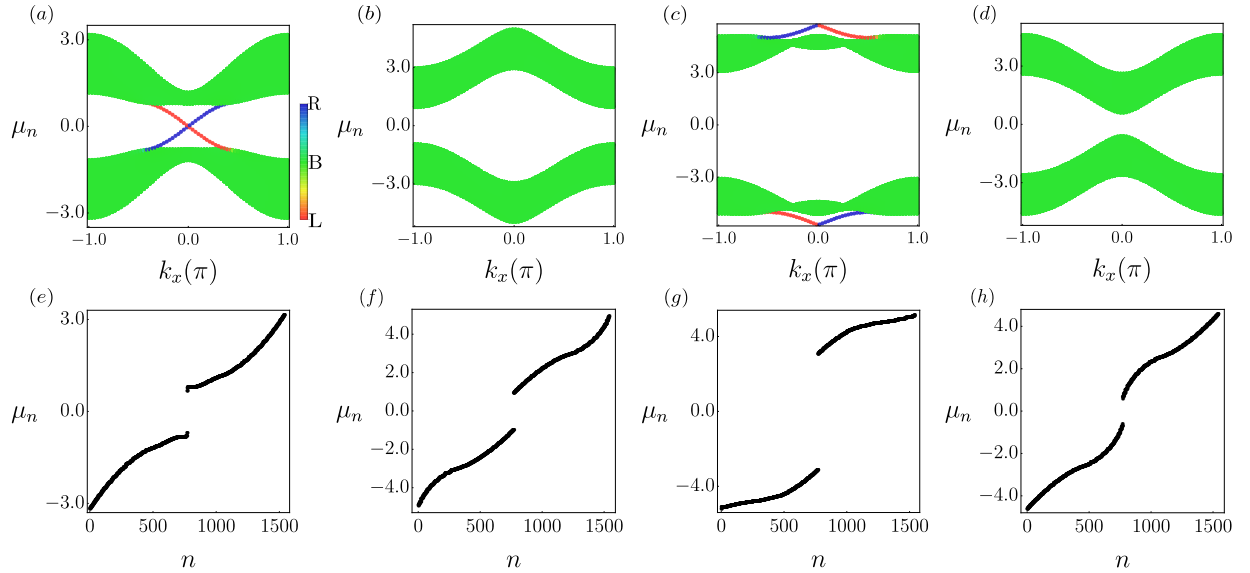
Figure S3: Quasienergy (μ_n) spectra in the high frequency ($\omega = 11.51$) regime for (a) Floquet topological insualtor (FTI) with the Chern number $C = -1$ (when drive amplitude $m_1 = -1.0$), (b) trivial insulator with $C = 0$ (when $m_1 = -3.25$), (c) FTI with $C = +1$ (when $m_1 = -4.14$), and (d) trivial insulator $C = 0$ (when $m_1 = -6.5$). FTI with $C = -1(+1)$ supports edge modes at $k_x = 0$ at Floquet zone center (boundary), while the $C = 0$ Floquet insulators are completely devoid of any edge mode. Corresponding quasienergy spectra in a periodic system with an edge dislocation-antidislocation pair in (e)-(f) show that these phases do not support any dislocation mode, since the Floquet-Bloch band inversion either takes place only at the Γ point of the BZ (for $C = \pm 1$) or there is not band inversion at all (for $C = 0$). Here blue and red [green] states are localized on the right (R) and left (L) edges [in the bulk (B)] of the system, respectively.

Supplementary Note 4.   FLOQUET TOPOLOGICAL INSULATORS WITH $C = \pm 1$ AT MEDIUM AND LOW FREQUENCIES

In the high frequency regime ($\omega \gtrsim 8$), as shown in Fig. 2 of the main text, the Floquet insulators can be either topological with $C = \pm 1$ or trivial with $C = 0$. Specifically, the $C = +1$ FTI is qualitatively similar to the one found in a static system [see Sec. Supplementary Note 1 and Fig. S1]. For example, it features zero quasienergy normal dislocation modes at the Floquet zone center as the associated Floquet-Bloch band inversion takes place at the M point of the BZ [see Fig. 3 of the main text]. Moreover, the $C = 0$ Floquet insulator in the high-frequency regime is devoid of any dislocation modes, as in the static system. By contrast, the $C = -1$ FTI supports anomalous dislocation mode at the Floquet zone boundary [see Fig. 3 of the main text], which does not have any analogue in the static system.

By contrast, even though in the medium and low frequency regimes, we find the Floquet insulating phases with $C = \pm 1$ and 0 [Fig. 2], they are quite different than the ones occupying the high frequency regime. For example, as shown in the main text [see Fig. 5], a Floquet insulator with $C = 0$ can feature edge modes at Floquet zone center and boundary at the Γ and M points. The edge modes near the M point are ultimately responsible for the normal and anomalous dislocation modes, respectively residing at the Floquet zone center and boundary. The Chern number $C = 0$ in such a phase can be reconciled with the fact that in Floquet insulators $C = C_{\mathrm{ZC}} - C_{\mathrm{ZB}}$, where C_{ZC} (C_{ZB}) is the Chern number at the Floquet zone center (boundary). For the above mentioned $C = 0$ phase, we find that $C_{\mathrm{ZC}} = C_{\mathrm{ZB}} = 0$, as it features Floquet-Bloch band inversion at both Γ and M points at Floquet zone center and boundary. Note that such a $C = 0$ Floquet insulator, which we name the π-trivial insulator, as well as the ones with $C = \pm 2$ bear no analogues in static system. Even though we cannot rule out the possibility of a $C = 0$ Floquet insulator with $C_{\mathrm{ZC}} = C_{\mathrm{ZB}} = \pm 1$, the model we study here does not show such phases down to frequency $\omega = 1.5$.

The fact that in a time-reversal symmetry breaking Floquet insulator the net Chern number (C) accounts for the contributions arising from the Flqouet zone center (yielding C_{ZC}) and its boundary (yielding C_{ZB}), with $C = C_{\mathrm{ZC}} - C_{\mathrm{ZB}}$, opens up various possibilities to realize a net $C = \pm 1$ FTIs, without any analogues in a static system. Here we discuss two such possibilities, and refer to the phase diagram shown in Fig. 2 of the main text and Fig. S4. Note that a $C = +1$ FTI can be realized when $C_{\mathrm{ZC}} = 1$ and $C_{\mathrm{ZB}} = 0$. While $C_{\mathrm{ZC}} = 1$ results in the edge modes near $k_x = \pi$ at the Floquet zone center, we find edge modes near $k_x = 0$ and π at the Floquet zone boundary, yielding
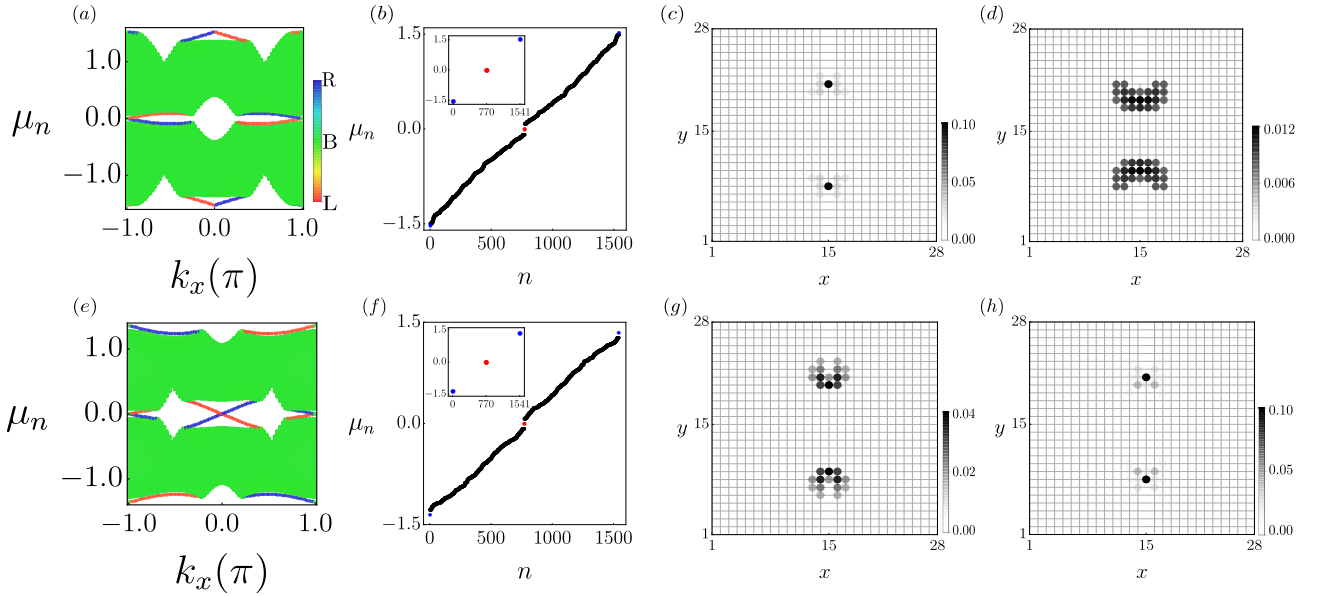
Figure S4: Dislocation as a bulk probe of FTIs with $C = +1$ [(a)-(d)] and $C = -1$ [(e)-(h)] at low frequencies. (a) Quasienergy (μ_n) spectra in a semi-infinite system (with k_x as a good quantum number) of linear dimension $L = 100$ in the y direction (with open boundaries) for drive frequency $\omega = 3.05$, amplitude $m_1 = -7.03$, $t_1 = t_0 = 1.0$ and $m_0 = 3.0$ [see Eq. (S1)]. Here blue and red [green] states are localized on the right (R) and left (L) edges [in the bulk (B)] of the system, respectively. (b) Normal (red) and anomalous (blue) dislocation modes, separated from the bulk states (black) by finite energy gaps. Corresponding local density of states (LDoS) for the (c) normal and (d) anomalous dislocation modes. Panels (e)-(f) are identical to panels (a)-(d), however for a FTI with $C = -1$ realized for $\omega = 2.72$, $m_1 = -4.46$, $t_1 = t_0 = 1.0$ and $m_0 = 3.0$.

$C_{\mathrm{ZB}} = 0$. This situation is demonstrated in Fig. S4(a). According to the $\mathbf{K} \cdot \mathbf{b}$ rule, such as phase then features both normal and anomalous dislocation modes, shown in Fig. S4(b)-(d). The dislocation modes solely arise from the edge modes near $k_x = \pi$. The situation for the $C = -1$ FTI is exactly the opposite [see Fig. S4(e)], which also supports both normal and anomalous dislocation modes, see Fig. S4(f)-(h). A detailed list of translationally active Floquet insulators, which may or may not have any counterpart in static system is presented in Table S1.

Supplementary Note 5. DISLOCATION MODES WITH DIFFERENT DRIVE PROTOCOLS

In the main manuscript, we considered a specific drive protocol [see Eq. (3) of the main text] and established that translationally active FTIs, featuring Floquet-Bloch band inversion at finite momentum, can be identified from the normal and anomalous dislocation modes, respectively found at quasienergies 0 (at Floquet zone center) and $\pm\omega/2$ (at Floquet zone boundaries). However, these conclusions are qualitatively insensitive to the specific choice of the drive protocol, and only depend on the $\mathbf{K} \cdot \mathbf{b}$ rule. Here, in particular, we consider two drive protocols, which are different from the one shown in Eq. (3) of the main text, namely (1) a step drive and (2) a sinusoidal drive, to anchor this claim.

(1) The drive protocol for a step drive assumes the following profile

$$
\begin{aligned}
V(t) & = m_1\sigma_3 \quad \text{for} \quad nT < t < nT + T/4 \\
& = m_2\sigma_3 \quad \text{for} \quad nT + T/4 < t < nT + 3T/4 \\
& = m_3\sigma_3 \quad \text{for} \quad nT + 3T/4 < t < (n+1)T,
\end{aligned} \tag{S8}
$$

where n is an integer and T is the period of the drive, also known as the stroboscopic time. For such a drive protocol it is quite challenging to express the effective Floquet Hamiltonian ($\hat{h}_{\mathrm{Flq}}(\mathbf{k})$) compactly. Nevertheless, we compute the chiral edge modes in the presence of such a drive in a semi-infinite system with k_x as a good quantum number to identify translationally active FTIs with the band inversion at the M point of the BZ (yielding chiral edge modes at $k_x = \pi$), that can take place either at the Floquet zone center, yielding normal dislocation mode at quasienergy $\mu = 0$, or at the Floquet zone boundary, yielding anomalous dislocation mode at quasienergies $\mu = \pm\omega/2$. In addition, we also identify the π-trivial insulator that simultaneously supports normal and anomalous dislocation
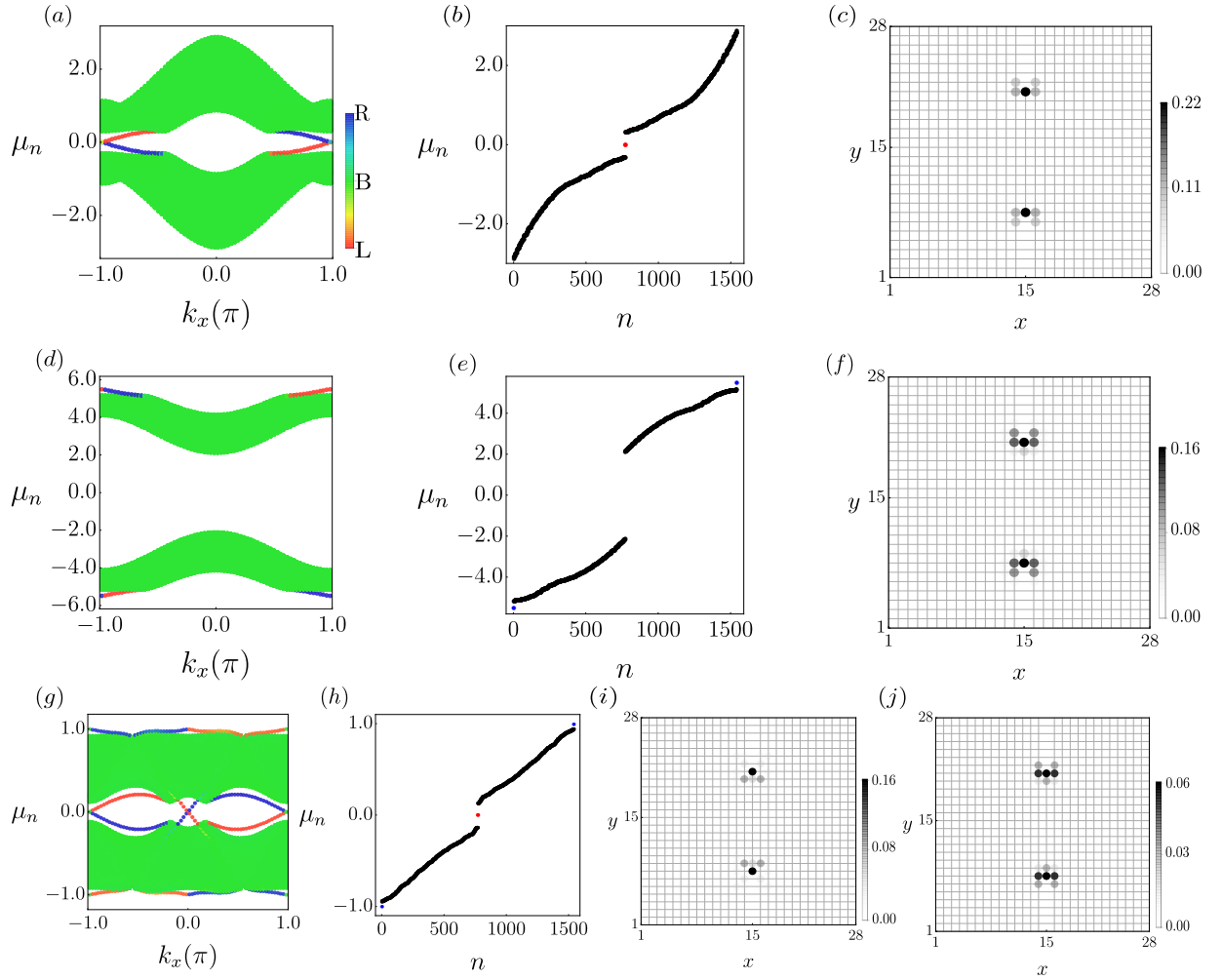
Figure S5: First column: Chiral edge modes for drive frequency $\omega = 6.0$ (first row), $\omega = 11.0$ (second row) and $\omega = 2.0$ (third row) for a step drive with drive amplitude $m_1 = 3.0$, $m_2 = -11.0$ and $m_3 = -8.5$ (first and second row), and $m_1 = m_3 = 2.4$ and $m_2 = -2.8$ (third row) (see Eq. (S8) for details) in a semi-infinite system with k_x as good quantum number. Second column: Corresponding quasienergy (μ_n) spectra in the presence of a pair of edge dislocation-antidislocation in periodic systems. Third column: Local density of states (LDoS) associated with the normal (first row) and anomalous (second row) dislocation modes. The LDoS for the normal and anomalous dislocation modes in a π-trivial insulator are respectively shown in the third and fourth column of the third row. Throughout we set $m_0 = 0.0$ in the static Hamiltonian. Here blue and red [green] states are localized on the right (R) and left (L) edges [in the bulk (B)] of the system, respectively.

modes. The results are displayed in Fig. S5 and they are in agreement with the $\mathbf{K} \cdot \mathbf{b}$ rule.

(2) Next we consider a sinusoidal drive for which

$$V(t) = m_1 \sigma_3 \, \sin(\omega t), \tag{S9}$$

where m_1 and ω respectively denote the amplitude and frequency of the sinusoidal drive, and $T = 2\pi/\omega$ is its period or the stroboscopic time. For the sake of simplicity, let us first consider a two-component wave function $(c_1(t) \ c_2(t))^\top$, which can be obtained by numerically solving the time-dependent Schrödinger equation

$$i \begin{pmatrix} \dot{c}_1 \\ \dot{c}_2 \end{pmatrix} = \hat{h}(t) \begin{pmatrix} c_1 \\ c_2 \end{pmatrix}, \tag{S10}$$

where $\dot{c}_j = \partial c_j / \partial t$ and $\hat{h}(t)$ is the time-dependent Hamiltonian that contains both time-independent static Hamiltonian as well as the time-dependent part, such as the one shown in Eq. (S9). Starting from the initial state $(1 \ 0)^\top$ we
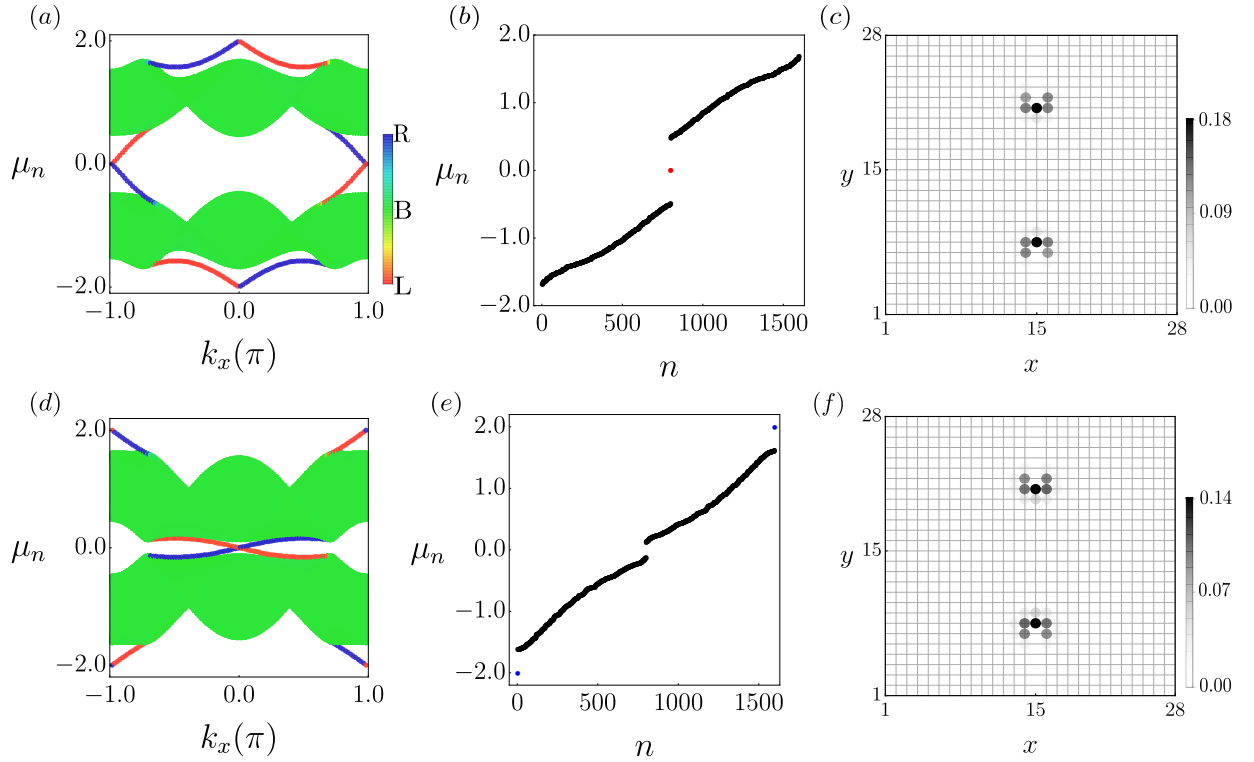
Figure S6: First column: Chiral edge modes for FTIs, obtained in the presence of a sinusoidal drive [see Eq. (S9)] in a semi-infinite system with k_x as a good quantum number for drive frequency $\omega = 4.0$, amplitude $m_1 = 2.0$ and $m_0 = -1.5$ (upper row), and $\omega = 4.0$, $m_1 = 2.5$ and $m_0 = -3.5$ (lower row). Second column: Corresponding quasienergy (μ_n) spectra in the presence of a pair of edge dislocation-antidislocation in periodic systems, supporting the normal (upper row, in red) and anomalous (lower row, in blue) dislocation modes. Third column: Corresponding local density of states. Here blue and red [green] states are localized on the right (R) and left (L) edges [in the bulk (B)] of the system, respectively.

numerically solve Eq. (S10) to obtain the normalized solution at time $t = T$ after a complete period, schematically given by $(c_1(T) \ c_2(T))^\top$. Similarly, starting from the initial state $(0 \ 1)^\top$, we obtain an orthonormal solution $(-c_2^\star(T) \ c_1^\star(T))^\top$. From these two solutions we then construct the Floquet operator

$$U(T) = \begin{pmatrix} c_1(T) & -c_2^\star(T) \\ c_2(T) & c_1^\star(T) \end{pmatrix}. \tag{S11}$$

By construction, the Floquet operator satisfies the initial condition $U(0) = \mathbf{I}_{2\times 2}$, where $\mathbf{I}_{2\times 2}$ is a two-dimensional identity matrix. This formalism can now be generalized to N-dimensional Hamiltonian (with arbitrary $N > 2$), which we solve numerically to find the response of FTIs in the presence of dislocations, when the system is under a sinusoidal drive, see Eq. (S9). The results are displayed in Fig. S6. With the sinusoidal drive we find FTIs with both normal and anomalous dislocation modes, in agreement with the $\mathbf{K} \cdot \mathbf{b}$ rule.

Supplementary Note 6.   THE $\mathbf{K} \cdot \mathbf{b}$ RULE AND MULTIPLE DISLOCATION MODES

Finally, we discuss the response of a Floquet topological insulator to dislocation, when specifically it supports more than one counter propagating one-dimensional topological edge modes at $k_x = \pi$ at the Floquet zone center and/or zone boundary. For the sake of concreteness we consider the drive protocol from Ref. [2], given by

$$H(\mathbf{k}, t) = \begin{cases} H_1(\mathbf{k}) = 3t_1 \sin(k_x) & \text{for} \quad nT < t < nT + T/3 \\ H_2(\mathbf{k}) = 3t_2 \sin(k_y) & \text{for} \quad nT + T/3 < t < nT + 2T/3 \\ H_3(\mathbf{k}) = 3t_3 \left[m_0 + t_0 \left\{\cos(k_x) + \cos(k_y)\right\}\right] & \text{for} \quad nT + 2T/3 < t < (n+1)T, \end{cases}$$

$(C_{\mathrm{ZC}}, C_{\mathrm{ZB}}, C)$	Chiral edge modes at	Edge modes	Dislocation	Existence	(m_1, ω) in Fig. 2
$(0, 0, 0)$	$k_x = 0, \pi$ at ZC	2	✓⊗	Not in HF and MF	−
$(0, 0, 0)$	$k_x = 0, \pi$ at ZB	2	✓⊕	Not in HF and MF	−
$(-1, -1, 0)$	$k_x = 0$ at ZC and $k_x = 0$ at ZB	2	✗	YES	$(-10.0, 11.0)$
$(1, 1, 0)$	$k_x = \pi$ at ZC and $k_x = \pi$ at ZB	2	✓⊕	Not in HF and MF	−
$(0, 0, 0)$	$k_x = 0, \pi$ at ZC and $k_x = 0, \pi$ at ZB	4	✓⊙	YES	$(-4.5, 1.94)$
$(1, 0, 1)$	$k_x = \pi$ at ZC	1	✓⊗	YES	$(-1.8, 12.9)$
$(0, -1, 1)$	$k_x = 0$ at ZB	1	✗	YES	$(-4.5, 10.0)$
$(1, 0, 1)$	$k_x = 0, \pi$ at ZB and $k_x = \pi$ at ZC	3	✓⊙	YES	$(-7.0, 3.0)$
$(0, -1, 1)$	$k_x = 0, \pi$ at ZC and $k_x = 0$ at ZB	3	✓⊗	YES	$(-9.0, 2.8)$
$(0, 1, -1)$	$k_x = \pi$ at ZB	1	✓⊕	YES	$(-5.3, 11.0)$
$(-1, 0, -1)$	$k_x = 0$ at ZC	1	✗	YES	$(-7.5, 10.0)$
$(0, 1, -1)$	$k_x = 0, \pi$ at ZC and $k_x = \pi$ at ZB	3	✓⊙	YES	$(-4.5, 2.7)$
$(-1, 0, -1)$	$k_x = 0$ at ZC and $k_x = 0, \pi$ at ZB	3	✓⊕	YES	$(-5.7, 2.8)$
$(1, -1, 2)$	$k_x = \pi$ at ZC and $k_x = 0$ at ZB	2	✓⊗	YES	$(-6.0, 4.0)$
$(-1, 1, -2)$	$k_x = 0$ at ZC and $k_x = \pi$ at ZB	2	✓⊕	YES	$(-9.0, 4.0)$

Table S1: First column: All possible combinations of $(C_{\mathrm{ZC}}, C_{\mathrm{ZB}}, C)$, with $C = C_{\mathrm{ZC}} - C_{\mathrm{ZB}}$, where $C_{\mathrm{ZC}}(C_{\mathrm{ZB}})$ is the Chern number arising from the Floquet zone center (boundary), yielding Floquet insulators with the total Chern number $C = 0$ (the first five rows), $+1$ (from the sixth to the ninth row), -1 (from the tenth to the thirteenth row), $+2$ (the second last row) and -2 (the last row). Second column: Corresponding momentum of the chiral edge modes in a semi-infinite system with k_x as the good quantum number, at the Floquet zone center (ZC) and/or zone boundary (ZB). The momentum of the chiral edge modes stems from the band inversion momentum. For example, edge modes at $k_x = 0$ and π respectively stem from the band inversion at the Γ and M points, which can take place at the Floquet ZC and/or ZB. Third column: Total number of edge modes of a given Floquet insulator. Fourth Column: Response of Floquet insulators to edge dislocation. Here, ✓(✗) corresponds to whether a phase supports (does not supoprt) dislocation modes. The symbol $\otimes$ ($\oplus$) stands for dislocation modes localized at Floquet ZC (ZB), while the phases simultaneously supporting dislocation modes at Floquet ZC and ZB are marked by $\odot$. Fifth column shows whether we find such a phase with a periodic kick, shown in Eq. (3) of the main text. Here, HF (MF) stands for high-frequency (medium-frequency). Sixth column: Parameter values (m_1, ω) yielding a specific phase, appearing in Fig. 2 of the main text, when $m_0 = 3.0$. Here, $m_1(\omega)$ is the amplitude (frequency) of the periodic kick. Note that Floquet insulators with identical Chern number (C) and total number of edge modes, set by the "dynamic winding number" from Ref. [1], can be completely different in nature, which can be probed by dislocations. See, for example, $C = \pm 1$ FTIs.

after setting the lattice spacing $a = 1$, where n is an integer. This is an example of a step drive, where the hopping along the x direction t_1 is only activated in the first one-third of each period. In the intermediate one-third interval of each cycle, only the hopping along the y direction t_2 is operative. In the final third of each period, a hopping $t_0 t_3$ in the x and y directions, and an onsite staggered potential $m_0 t_3$ are functioning. Therefore, over a full period the Floquet operator takes the following form [2]

$$U(\boldsymbol{k}, T) = \exp\left(\frac{-iH_3(\boldsymbol{k})T}{3}\right) \exp\left(\frac{-iH_2(\boldsymbol{k})T}{3}\right) \exp\left(\frac{-iH_1(\boldsymbol{k})T}{3}\right). \tag{S12}$$

The results for a specific choices of various parameters appearing in $H(\mathbf{k}, t)$ in Eq. (S12) are displayed in Fig. S7.

Fig. S7 shows that for the above chosen form of the drive protocol form Eq. (S12) and a specific choice of the drive parameters, the resulting Floquet insulator supports one pair of counter propagating edge mode near $k_x = \pi$ at the Floquet zone center and two pairs of counter propagating edge modes at $k_x = \pi$ at the Floquet zone boundaries. Therefore, by generalizing the proposed $\mathbf{K} \cdot \mathbf{b}$ rule, we expect such a Floquet insulator to support one normal dislocation mode at quasienergy $\mu = 0$ and two anomalous dislocation modes at quasienergies $\mu = \pm\omega/2$, respectively at the Floquet zone center and boundary. Our numerical simulation confirms these predictions. The dislocation modes are well separated from the bulk states and they are highly localized around the dislocation core. This
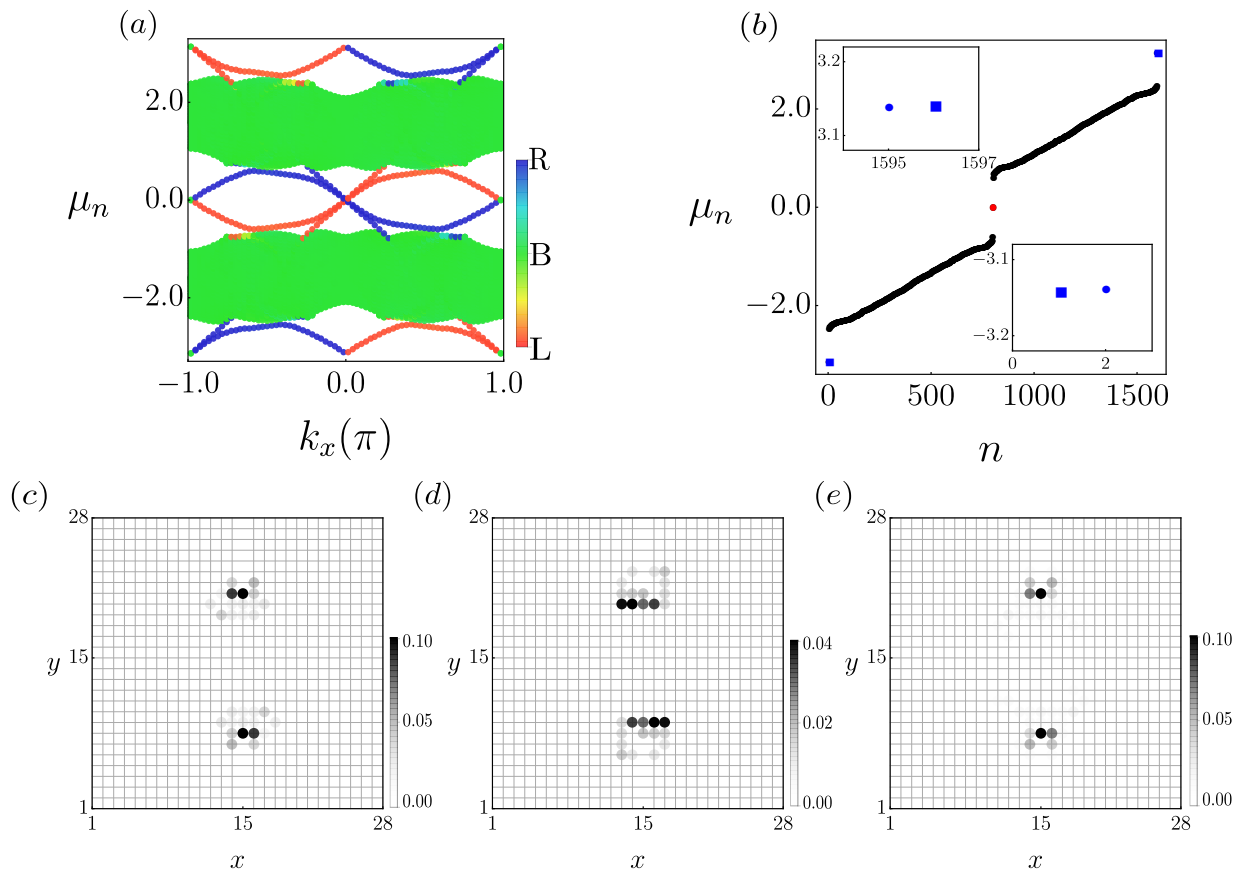
Figure S7: (a) Quasienergy spectra in a semiminfinite system with linear dimension $L = 100$ in the y direction for the drive protocol shown in Eq. (S12) with the conserved momentum k_x for $t_1 = t_2 = \pi/3$, $m = t_0 = 1$, $t_3 = 3\pi/2$. The blue [red] states reside on the right (R) [left (L)] edge, while the ones shown in green are localized in the bulk (B). (b) Quasi-energy spectra in a periodic system with an edge dislocation-antidislocation pair for the same drive protocol and set of parameters. Here solid blue circles and solid blue squares represent two particle-hole pairs of dislocation quasimodes residing at the Floquet zone boundary, and the solid red circle denote the near zero quasienergy particle-hole pair of dislocation quasimodes. The bulk states are shown in black. Local density of states (LDoS) for (c) normal dislocation mode (solid red circle), (d) one set of anomalous dislocation modes (solid blue square), (e) the other set of anomalous dislocation mode (solid blue circle).

observation can be generalized to further extend the jurisdiction of the proposed $\mathbf{K} \cdot \mathbf{b}$ rule for dislocation modes. In a given Floquet insulator, for each pair of counter propagating one-dimensional chiral edge modes at finite momentum, there exists one dislocation mode in the bulk of the system at the corresponding quasienergy.

Supplementary References

[1] Rudner, M. S., Lindner, N. H., Berg, E. & Levin, M., Anomalous Edge States and the Bulk-Edge Correspondence for Periodically Driven Two-Dimensional Systems, *Phys. Rev. X* **3**, 031005 (2013).

[2] Umer, M., Bomantara, R. D. & Gong, J., Counterpropagating edge states in Floquet topological insulating phases, *Phys. Rev. B* **101**, 235438 (2020).